Chapter 1

Ab-Initio Modeling of Lubricant Reactions with a Metal Al (111) Surface

Jun Zhong

Additional information is available at the end of the chapter

http://dx.doi.org/10.5772/intechopen.72512

Abstract

In this chapter, to assist the design of aluminum processing, density functional theory is utilized to depict optimal adsorption geometries on an Al (111) surface for two commonly used boundary-layer lubricant additives: vinyl-phosphonic and acetic acids, i.e., tri-bridged, bi-bridged, and uni-dentate coordinations of these adsorbates are examined to determine the optimal binding sites on the surface. During these static analyses, charge density of states for molecular oxygen ions reacting with Al ions in the surface is applied to revealing the evolution essentials of molecular binding strength on surface. In addition, ab-initio molecular dynamics based upon density functional theory is employed to probe dynamic decomposition pathways on the Al (111) surface for two other important boundary-layer lubricant additives: butanoic acid and butanol alcohol. These decomposition pathways may occur upon molecular collisions with the surface, leading to formation of molecular pieces adhering on surface. Simulations are found to be in qualitative accord with existing experimental observations.

Keywords: density functional theory, ab-initio molecular dynamics, vinyl-phosphonic acid, acetic acid, butanoic acid, butanol alcohol, Al (111) surface

1. Introduction

Lubricant formulations used to control friction and wear in metallic forming processes typically contain mixtures of molecular additives in the base oil. Common lubricant additives in the metal-rolling processes consist of one or more aliphatic alcohols, acids or esters such as vinyl-phosphonic acid, acetic acid, butanoic acid and butanol alcohol etc. which have hydroxyl (OH) or carboxyl (O═C─OH) functional group [named oxygen-rich base (O-base)] to behave like a cationic anchor with electron-rich charges [1–3]. Initially, these molecules are

thought to anchor onto metal (e.g., hydroxide-alumina) surfaces through their O-bases. And then, such O-bases are believed to decompose on fresh (pure aluminum) surfaces occurring in the actual rolling work. As a result, these adsorbed and decomposed molecular pieces will contribute to the boundary thin-film lubrication and protection, i.e., their residual fragments (e.g., molecular chain tails) adhered on fresh surfaces with several molecular layers thick may serve as corrosion inhibitors of surface.

For adsorbate examples, **Figure 1** shows an illustration of two molecular structures: a vinyl-phosphonic acid [VPA, $H_3C_2P(O)(OH)_2$] with a tri-podal O-base [2(OH)─P═O] plus a vinyl-hydrocarbon tail [4] as shown in **Figure 1(a)**, and an acetic acid [EA, $H_3C_2(O)(OH)$] with an alkyl-chain plus a bi-podal O-base [O═C─OH] as shown in **Figure 1(b)**.

In **Figure 1(a)**, a study of the inelastic tunneling spectroscopy (IETS) for a VPA adsorption on a hydroxide-Al_2O_3 (0001) surface implied that the vinyl-tail on VPA did not participate in bonding to the oxide surface [5], but left itself accessible to react with other general lubricant molecules, which may serve as a molecular cap on the surface to inhibit migrations of corrosive species into the oxide surface. This reaction usually resulted in a tri-dentate coordination for the VPA on surface through a tri-podal O-base even if such a tri-dentate coordination was not unique on surface [6]. Crowell et al. utilized the electron energy loss spectroscopy (EELS) to observe an EA adsorption on an Al (111) surface starting at a very low temperature of 120 K [7]. They observed that a symmetrically bi-bridged geometry of main piece decomposed from the EA was more likely to bond to the surface than other configurations. In brief, both of above studies found that O-bases on acid molecules may usually bond to aluminum/alumina surfaces and oxidize them prior to other twigs, and then had molecular residual fragments (molecular chain tails) form thin-film inhibitors on the surfaces.

In addition, Underhill and Timsit [8] applied the X-ray photoelectron spectroscopy (XPS) to the study of dynamic decomposition pathways for 1-butanol and propanoic acid through molecular collisions with a clean Al (111) surface. At room temperature (e.g., 300 K), their results suggested that acid molecules break up on the surface, leading to attachments of aliphatic chains via their O-bases on surface. Alternatively, aliphatic alcohols were found to react with Al ions in the surface via their O-bases alone. At elevated temperatures (about 400 K), both acid and alcohol were found to dissociate on the clean surface, leading to attachments of aliphatic chains via their end C ions and pieces of decomposed O-base on surface, to form molecular boundary thin-films of surface. However, such the dynamic decomposition has received minimal attention in the literature.

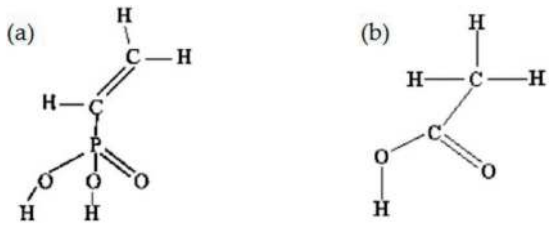

Figure 1. Two acid molecules: (a) a VPA molecule; (b) an EA molecule.

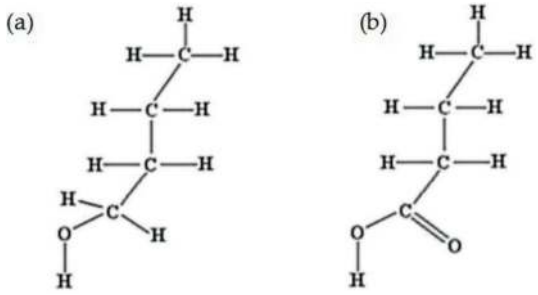

Figure 2. Schematics of (a) a butanol molecule; (b) a butanoic molecule.

In **Figure 2**, two lubricant additives, butanol alcohol [$H_3C{-}(CH_2)_2{-}H_2C{-}(OH)$] and butanoic acid [$H_3C{-}(CH_2)_2{-}C(O)(OH)$], are shown schematically: the alcohol in **Figure 2(a)** has a C─OH functional group; while the acid in **Figure 2(b)** has an O═C─OH functional group which is very similar to the EA as shown in **Figure 1(b)**.

In this chapter, we carry out series of density functional (DFT) analyses on how two commonly used boundary-layer lubricant additives, VPA and EA, bond statically to a clean (pure) Al (111) surface in their optimal geometries. During the actual rolling (forming) processes to hydroxide-alumina surfaces, since top textures (layers) of the surfaces are usually peeled off so that fresh (pure) aluminum surfaces (below top layers) with nascent islands can be subsequently exposed in the air, without loss of generality, such the DFT static outputs may help powerfully determine the favorably bonding mechanisms of additives to the highly reactive islands on fresh surfaces, so as to make clear the formation of protective thin-film on alumina surfaces. Then next, we examine dynamic decomposition pathways on the clean Al (111) surface using ab-initio molecular dynamics (AIMD) for two other important aliphatic boundary-layer lubricant additives: butanol alcohol and butanoic acid, to determine their thermal mechanisms of monolayer formation on the surface. During the AIMD simulation, each molecule is orientated to collide with the clean surface through its reactive O-base. Initial approaching speeds of molecules toward the surface are taken from the actual Al-rolling process. Decomposition pieces of additive molecules on the Al (111) surface are explored in details throughout the whole simulation. Simulation outputs are qualitatively compared with experimental observations using the EELS and the XPS for similar molecules [7, 8], which may reveal some unknown decomposed configurations in a previous DFT static study [9].

2. Configurations of adsorbates and adsorbents

2.1. Adsorbate configurations

Figure 3 shows a side view of a VPA structure, along with isosurfaces of charge density with the electron (e^-) localization function (ELF) representing the probability of finding a second e^- with the same spin in the neighboring region of the first (reference) e^- within [0, 1]. In other

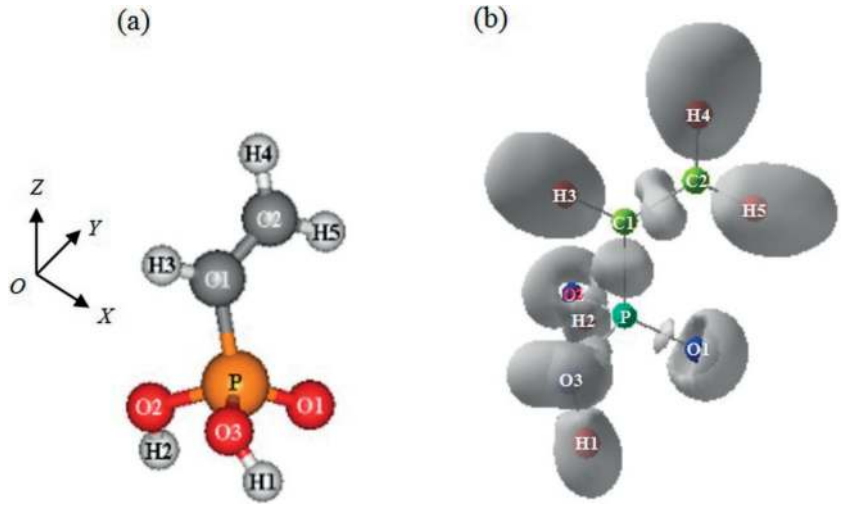

Figure 3. Side view of a VPA structure: (a) a vinyl-group and a tri-podal based P—O bonds on the VPA; (b) isosurfaces of charge density at the ELF = 0.81 for the VPA.

words, a high ELF value means a highly localized behavior for the first (reference) e^- [10–13]. According to this definition, high ELF values are typically associated with covalent bonds, e^- lone pairs, or inert cores [14]. In **Figure 3(b)**, ELF = 0.81 is the best visual difference of isosurfaces for each of atomic bonds according to comments in ref. [15]. The VASP (Vienna Ab-initio Simulation Package) calculations for the VPA indicated that two e^- lone pairs aggregated to O2 (and O3) nearby (a circle-lunar lobe) because of its *aniso-sp*^{3} hybrid bonding to H2 and P neighbors. However, O1 formed a weak double bond with P and had slightly more e^- lone pairs (a hemisphere lobe) than O2 and O3, see **Figure 5(a)**. In **Figure 3(a)**, such a VPA

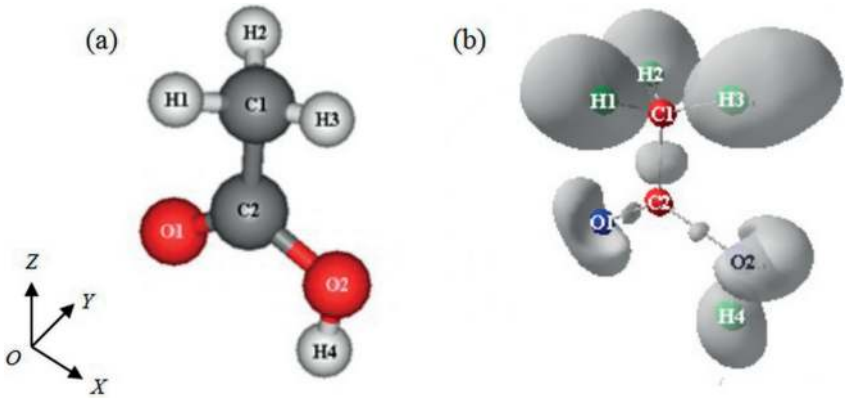

Figure 4. Side view of an EA structure: (a) a methyl group and a bi-podal-based C—O bonds on the EA; (b) isosurfaces of charge density at the ELF = 0.67 for the EA.

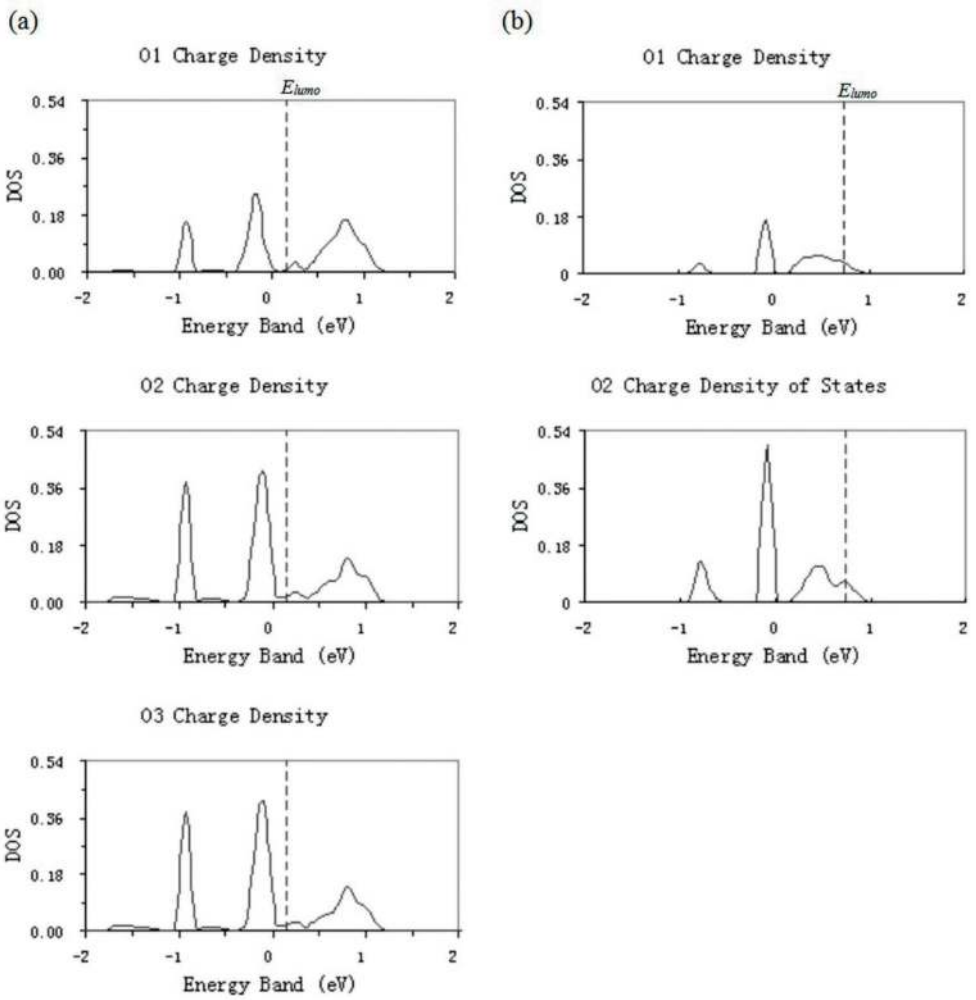

Figure 5. Charge density of states (DOS) for O ions on (a) the VPA and (b) the EA.

conformation was the most favorably energetic for the vinyl-group coplanar with the P═O1 double bond, and was consistent with that predicted in ref. [15]. Also, C1═C2 double bond showed an *aniso-sp*^{2} hybrid bonding type.

Figure 4 shows a side view of an EA structure, along with isosurfaces of charge density at the ELF = 0.67 to provide the best visual difference for each of atomic bonds. VASP analyses for the EA indicated that two e^- lone pairs aggregated to O2 nearby (a hemisphere lobe) because of its *aniso-sp*^{3} hybrid bonding to H4 and C2 neighbors. However, a strong C2═O1 double bond (an *aniso-sp*^{2} hybrid type) resulted in a lower charge density in e^- lone pairs around O1 (a cashew type) than around O2, see **Figure 5(b)**.

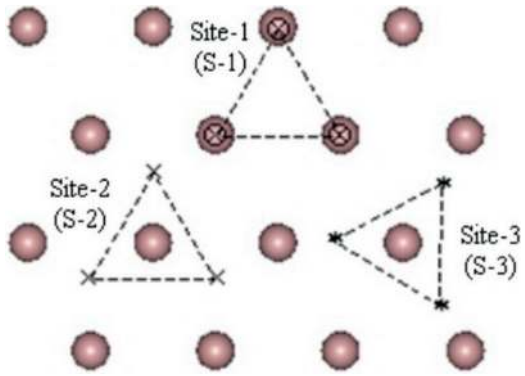

Figure 6. Three most favorable adsorption sites in top layer of Al (111) surface slab.

Figure 5 shows distributions of charge density of states (DOS) for three O ions on the VPA and two O ions on the EA, respectively. In **Figure 5**, the E_{lumo} represented the energy level corresponding to the lowest unoccupied molecular orbital, i.e., above the E_{lumo} the DOS for O ions represented unoccupied states. In **Figure 5**, more portions of the DOS for O ions on the VPA appeared in orbitals above the E_{lumo} than those on the EA, implying that VPA may be more reactive with the Al surface than EA by feat of their O ions.

2.2. Adsorbent configurations

Since Al (111) surface has the lowest surface energy among all surface geometries in aluminum bulk, it is likely to expose in the air during the actual rolling process. So here it is selected as an adsorption slab surface (adsorbent) to react with above adsorbates. **Figure 6** shows three distinguishable adsorption sites in the top layer of Al (111) surface slab. We refer to them as site-1, -2, and -3, respectively. Among these sites, site-1 (S-1) had corners at three Al ions; site-2 (S-2) had corners at three cave points (cross signs); and site-3 (S-3) had corners at three saddle points (ice-star signs). According to past experiences [14], these three sites were more likely to react with adsorbates than others because they allowed O-bases on adsorbates to bond to surface stronger than other ones.

3. Simulation methodologies and procedures

3.1. Static calculations

These calculations were based upon the DFT [16–18] using the Vienna Ab-initio Simulation Package (VASP). At first, all calculations were performed using the Projector-Augmented Wave (PAW) pseudopotentials [19]. The GGA created by Perdew and co-workers [20, 21] was employed for evaluating the exchange-correlation energy. This methodology was similar to a previous study of optimizing the VPA adsorption geometries on an α-Al_2O_3 (0001) surface

[15]. Prior to these calculations, lattice constant, bulk modulus and cohesive energy for a pure aluminum bulk by fitting data of energy versus volume to the Murnaghan Eq. [22] was calculated. A regular Monkhorst-Pack grid [23] of 17 × 17 × 17 was chosen as the best *k*-point sampling, so that the total energy of system was converged within 1–2 meV/atom. The computed lattice constant, a_0'= 4.05(3) Å, see ref. [9].

Then next, calculations of acid adsorptions on the Al (111) surface slab were conducted in a supercell with a periodic four-layer $3a_0$'× $3a_0$'units (16 Al ions per layer) in XY directions. A plane-wave cutoff energy, 400 eV, which was primarily required by the "hardest ions (C and O)", was chosen. A regular Monkhorst-Pack grid of a 5×5×1 *k*-point sampling was selected for this orthogonal supercell with three definite orientations: $a[1\bar{1}0] = 2\sqrt{2}a_0$' along the X axis, $b[11\bar{2}] = \sqrt{6}a_0$' along the Y axis, and *c* [111] = 26.0 Å along the Z axis, plus a vacuum distance of 10.0 Å in *c* direction and with one bottom layer of the Al (111) slab fixed along *c* direction in the supercell. The atomic geometry was optimized through minimizing the Hellman-Feyman forces using a conjugate gradient algorithm [11], until the total force on each ion reduced to 0.05 eV/Å or less.

3.2. Dynamic simulations

In this study, all ab-initio molecular dynamics (AIMD) simulations were also based upon the DFT as implemented in the VASP. A Vanderbilt-type ultrasoft pseudopotentials (USP) were utilized for elemental constituents by means of the GGA [24]. In real practice, the GGA usually yielded inaccurate reaction barriers [25–27], while a semilocal-BLYP and hybrid-B3LYP functionals seemed to predict adsorption energies accurately and distinguish adsorption sites correctly. However, for the study of dynamic decomposition, we believed that the GGA was also a reasonable compromise since a highly colliding velocity acting on molecules toward the Al surface slab would likely overwhelm any barrier to the decomposition.

During the AIMD simulation, first of all, lattice constant (a_0) of pure Al bulk was calculated using the NPT ensemble, which thermally equilibrated one $2a_0 \times 2a_0 \times 2a_0$ unit cell at a room temperature (300 K) plus an ambient pressure of 1.0 bar for about 1500 time steps, a simulation time step of 0.001 ps was selected. A regular gamma-centered grid of 5 × 5 × 5 was chosen as the best *k*-point sampling for the unit cell. Total energy of the system was converged within 1–2 meV/atom. A plane-wave cutoff energy, 400 eV, as dictated by the hardest oxygen pseudopotential, was adopted in all simulations. The computed lattice constant, a_0 = 4.05(7) Å, was favorably fitting to other calculations and experimental observations [28].

Besides, for modeling interactions between additive molecules and an Al (111) slab, a Monkhorst-Pack grid of 5 × 5 × 1 was selected for the best *k*-point sampling. A supercell with the entire Al (111) slab consisted of four Al layers (36 ions per layer) of 144 ions. This orthorhombic geometry had three definite orientations: $a[1\bar{1}0] = \frac{3}{2}\sqrt{6}a_0$ along the X axis, $b[11\bar{2}] = 3\sqrt{2}a_0$ along the Y axis, and *c* [111] = 40.0 Å along the Z axis plus a vacuum distance of 24.0 Å in the *c* direction to preclude interactions with periodic images. The bottom layer of the Al (111) slab was fixed along the *c* direction to prevent the whole slab motion during impacts of additive molecules onto the Al slab surface.

In addition, each of isolated molecules was optimized in a same vacuum supercell as used for the Al (111) slab. And then, it was equilibrated at 300 K for about 1500 time steps by re-scaling thermal velocities at each time step [29], the time step = 0.001 ps. Simultaneously, the Al (111) slab were equilibrated in its supercell by the same technique as each isolated molecule. Then next, each isolated molecule was transferred into the simulation supercell containing the Al (111) slab, respectively.

After thermal equilibration, all AIMD simulations for interactions between additive molecules and the Al (111) slab were carried out through a constant energy method (NVE) without controlling temperature of system [29]. In real processing works, when steel rollers converged to form bite regions in the metal rolling of Al alloys, pressure gradients in bite regions would draw lubricant additives into conjunction. At this time, translational speeds acting on a single molecule can be estimated to reach as high as 2500 m/s due to kinematics at the tool/Al interface [30]. Hence, a serial approaching velocities, V_d, based upon this situation, were adopted in the AIMD simulations. Then next, each additive molecule started accelerating toward the Al (111) slab surface once it met a net attraction from the surface. To save computational cost, initial vertical spacing between each additive molecule and Al ions in the surface was set to 2.30 Å, which was slightly larger than Al—O bond length (1.86–1.97 Å) as indicated in ref. [31].

4. Results and discussions

4.1. Static calculations

To better understand adsorption mechanisms of VPA and EA on Al (111) surface, several combined adsorbate/slab systems were selected for the investigation. The adsorption enthalpy (the binding energy or the binding strength), $\Delta H_{ads}^{(m)}$, was defined as the difference between the total energy of the combined adsorbate plus slab (adsorbent), and the total energy of the separated adsorbate and, the separated slab, which was given by

$$\Delta H_{ads}^{(m)} = E(\text{adsorbate \& slab}) - [E(\text{adsorbate}) + E(\text{slab})] \quad (1)$$

where the superscript (m) indicated one reaction type. A negative $\Delta H_{ads}^{(m)}$ value corresponded to a favorable adsorption on surface, while a positive one represented an unlikely reaction on surface.

Preliminary investigation of the VPA adsorption on Al (111) surface indicated that, its standing geometries at S-2 and S-3 always shifted to S-1 on the surface when using the energy minimization. Similar results can be obtained for the EA adsorption at S-2 and S-3 on Al (111) surface. Therefore, S-1 was regarded as the most favorable adsorption site for these adsorbates. According to this, we would only focus on the S-1 for the VPA and the EA adsorptions on Al (111) surface.

4.1.1. Uni-dentate configurations

Figure 7 shows side views of VPA and EA adsorptions on Al(111) surface in their own uni-dentate coordination with one of their oxygen ions and one H ion (dissociated from this oxygen ion) bonding onto the surface, respectively. Molecular binding sites on the surface were both at S-1.

In **Figure 7**, Al—H and Al—O single bonds were formed on Al (111) surface to sustain the adsorbates. Adsorption enthalpies corresponding to **Figure 7(a)**, **(b)**, $\Delta H_{ads}^{(VPS,EA)} = -0.89$ and −0.51 eV, respectively. Moreover, VASP calculations indicated that each of adsorption enthalpies would bring additional negative values: −0.26 eV, due to subsequent formation of gaseous H_2 molecule by means of H ions desorbed from Al (111) surface. Therefore, if ignoring zero point energy corrections, the formation of gaseous H_2 molecule in these final adsorptions were more favorable to those individual H ions adsorbing onto the surface, so molecular main pieces would be left onto the surface alone in adsorption end, see **Figure 8**.

Figure 8 shows isosurfaces of charge density for vinyl-phosphonate and acetate on Al (111) surface in their own uni-dentate coordination, respectively. A value of the ELF = 0.67 was chosen because it may provide the best visual difference in charge density on C—O and P—O bonds. In **Figure 8(b)**, a small lobe can be observed on C2—O2 bond, while P—O3 bond in **Figure 8(a)** had no such a character. This meant that O_2 ion on C2—O2 bond was more covalent, while O3 ion on P—O3 bond was more ionic. This was expected because P was less electronegative than C (2.1 vs. 2.5), see ref. [32]. Therefore, during these two adsorptions, portions of charge density for O3 on vinyl-phosphonate in **Figure 8(a)** would move more toward the reacting Al ion in surface than that for O2 on acetate in **Figure 8(b)**. Qualitatively, this may occur reasonably because more unoccupied e^- states for O3 than those for O2 seemed to make the final binding state of VPA stabler than that of EA on the surface.

Quantitatively, **Figure 9(a)** shows the modified charge density of states (DOS) for O3 on vinyl-phosphonate as shown in **Figure 8(a)**, corresponding to e^- states (around the E_{lumo}) in **Figure 5(a)**. Comparing this DOS with that in **Figure 5(a)** for O3 on VPA, it may find that many of unoccupied e^- states evolved into occupied ones (below the E_F, the Fermi level on energy band) after VPA adsorption on surface. Similarly, **Figure 9(b)** shows the modified DOS for O2 on acetate as shown in **Figure 8(b)**, corresponding to e^- states (around the E_{lumo}) in **Figure 5(b)**. Comparing O3 on VPA with O2 on EA, we concluded that the DOS for O3 would shift more below the E_F than that for O2 after molecular adsorptions, which made the binding energy of VPA larger than that of EA.

In the following subsections, similar trends of the DOS curves in **Figure 9** can also be observed for O ions on molecular main piece reacting with Al (111) surface in bi-bridged (VPA and EA) and tri-bridged (VPA) coordinations. According to these results, we believed that the VPA should bind stronger than the equivalent EA on Al (111) surface because of its larger number of unoccupied e^- states available for bonding to the surface.

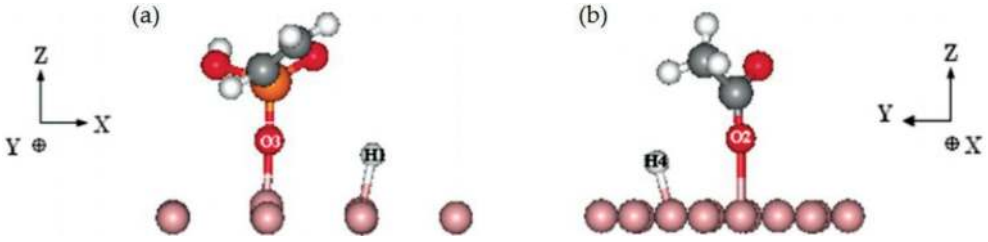

Figure 7. Side views of (a) VPA and (b) EA adsorptions on Al (111) surface in uni-dentate coordination.

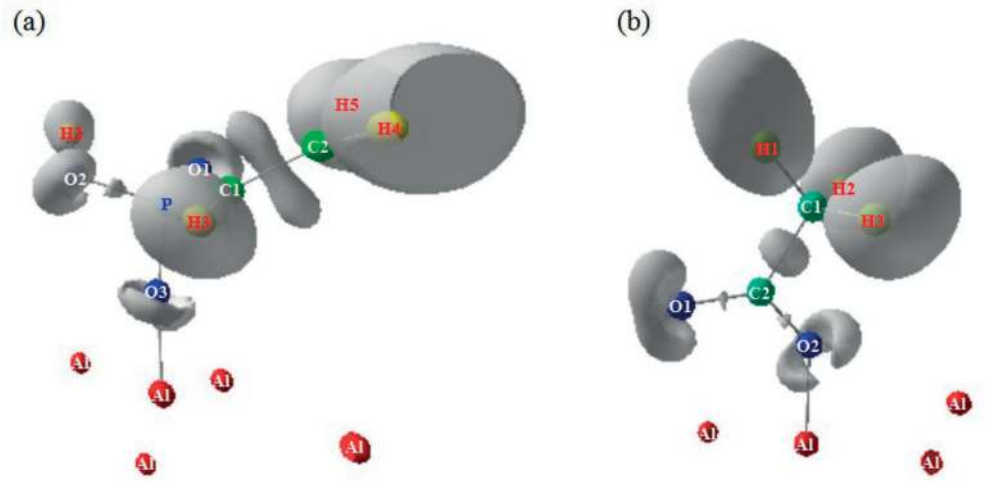

Figure 8. Isosurfaces of charge density at the ELF = 0.67 for (a) VPA and for (b) EA adsorptions on Al (111) surface in their own uni-dentate coordination.

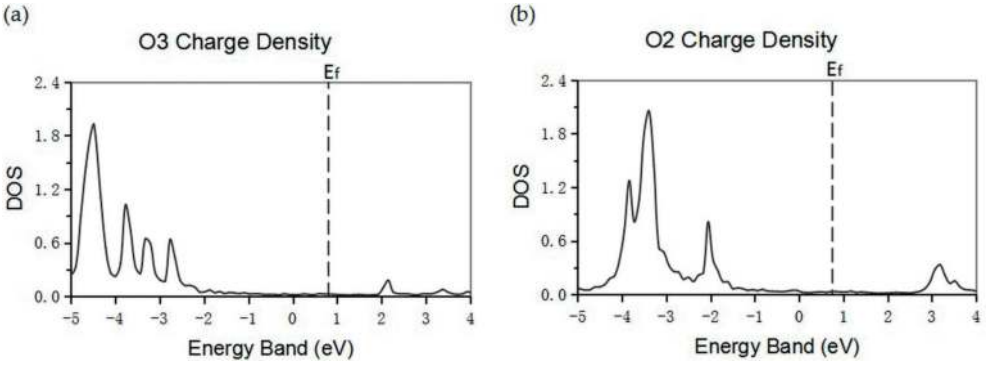

Figure 9. The modified DOS for (a) O3 ion on vinyl-phosphonate and (b) O2 ion on acetate.

4.1.2. Bi-bridged configurations

Figure 10 shows side views of vinyl-phosphonate and acetate adsorptions on Al (111) surface in their own bi-bridged coordination, respectively, with H ions liberating from molecular main piece and bonding to the surface. In these two adsorptions, adsorption enthalpies corresponding to **Figure 10(a)**, **(b)**, $\Delta H_{ads}^{(VPA,EA)} = -1.32$ and -1.52 eV, respectively. Moreover, subsequent formation of gaseous H_2 molecule by means of H ions desorbed from Al (111) surface would bring additional negative values for these enthalpies: -0.51 and -0.26 eV, respectively, indicating that both vinyl-phosphonate and acetate bonding to Al (111) surface alone in their own bi-bridged coordination, respectively, would be more favorable in final adsorptions.

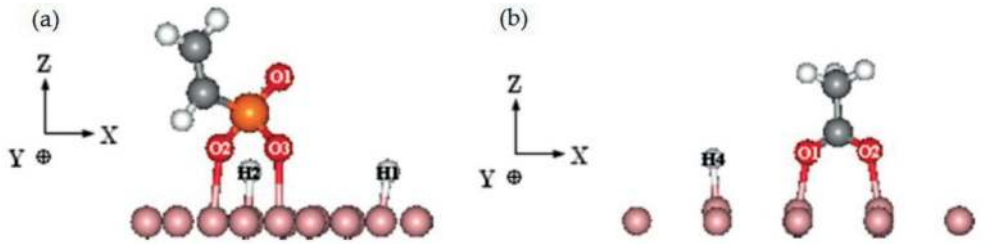

Figure 10. Side views of (a) vinyl-phosphonate and (b) acetate adsorptions on Al (111) surface in bi-bridged coordination, respectively.

4.1.3. Tri-bridged configurations

Figure 11 shows a side view of VPA adsorption on Al (111) surface in tri-bridged coordination. In **Figure 11**, 2 H ions liberated from the VPA main piece through the condensing reaction and were adsorbed on the surface. Adsorption enthalpy corresponding to **Figure 11**, $\Delta H_{ads}^{(VPA)} = -2.61$ eV. Moreover, subsequent formation of gaseous H_2 molecule by means of H ions desorbed from Al (111) surface would bring additional negative values for this enthalpy: −0.51 eV, indicating that vinyl-phosphonate bonding to Al (111) surface alone in its own tri-bridged coordination, would be more favorable in final adsorption.

4.1.4. Other adsorption geometries

When rotating initial configurations of adsorbates by some clockwise angels (e.g., 120° or 180° etc) toward Al (111) surface rather than their functional groups facing the surface, i.e., with the CH_3 end directly pointing toward the surface, the binding energies of adsorbates on the surface would indicate positive values, meaning that such kinds of reacting geometries were unfavorable in the adsorption.

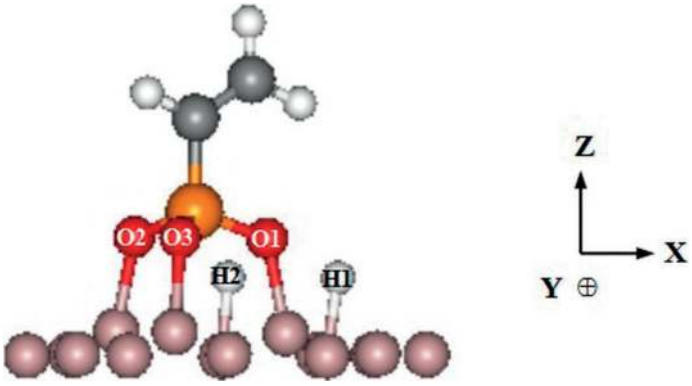

Figure 11. A side view of vinyl-phosphonate adsorption on Al (111) surface in tri-bridged coordination.

4.1.5. Conclusions

In summary, if ignoring entropy contributions, for the VPA, the best favorable adsorption geometries on Al (111) surface were in the order: tri-bridged coordination > bi-bridged coordination > uni-dentate coordination. While for the EA, the best adsorption geometries on Al (111) surface were in the order: bi-bridged coordination > uni-dentate coordination.

In addition, comparing these two adsorption types, in each of above adsorption geometries, the binding state of VPA on Al (111) surface was always stronger than that of equivalent EA on the surface. The main reason could be due to a more highly reactive 2(O)—P═O functional group with the surface than an O—C═O functional one. H ions liberating from molecular main pieces and adsorbing onto the surface, also influenced all of the binding states in above. However, the formation of gaseous H_2 molecules by means of H ions desorbed from the surface was more favorable in adsorption ends.

4.2. Dynamic simulations

In this section, dynamic decomposition pathways for two selected aliphatic boundary-layer lubricant additives: butanoic acid and butanol alcohol on Al (111) surface, are discussed using ab-initio molecular dynamics.

Corresponding to **Figure 2**, **Figure 12** shows isosurfaces of charge density at the ELF = 0.93 for these two molecules. In **Figure 12(a)**, O2 had two e^- lone pairs (a circular-lunar lobe) because of its *aniso-sp*^{3} hybrid bonding to C and H neighbors; O1 formed a strong double bond with C, leading to lower charge density (a semi-lunar lobe) than around O2; Both O1 and O2 behaved more reactive with the clean Al (111) surface than other ions on butanoic acid, which were very similar to those in **Figure 4(b)**. In **Figure 12(b)**, O2 also had two e^- lone pairs (a circular-lunar lobe) because of its *aniso-sp*^{3} hybrid bonding to C and H neighbors; O2 showed more reactive with the clean Al (111) surface than other ions on butanol alcohol. In a word, the ELF analyses indicated that functional groups O═C—OH and C—OH on these two molecules were electron-rich, and hence were more likely to react with the Al surface than other C—H and C—C twigs.

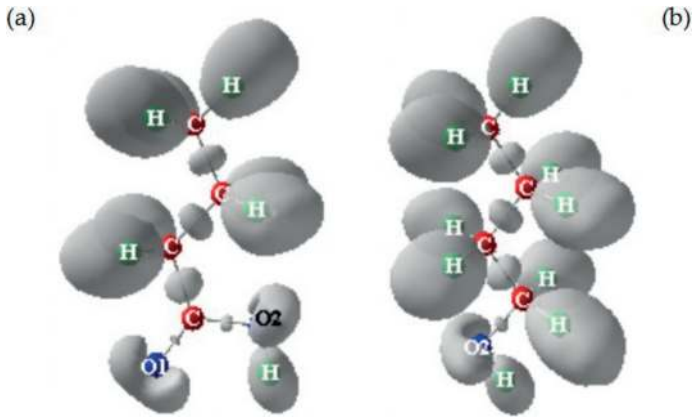

Figure 12. Side views of isosurfaces of charge density at the ELF = 0.67 for (a) butanoic acid and for (b) butanol alcohol.

Figure 13 shows initial geometries of butanoic acid and butanol alcohol interactions with Al (111) surface slab in four models. In each model, an additive molecule was positioned with its carbon backbone directly above the center of the equilibrated Al (111) surface, molecular orientations along [111] direction were shown in **Figure 13(a)–(d)**, respectively. In **Figure 13**, the first three models were for butanoic acid reactions with Al (111) slab surface: In model-1 (M−1), V_d = −15.0 Å/ps (1500 m/s) and the O ion on O═C bond was set at one 2.30 Å spacing above the Al (111) slab surface. In model-2 (M−2), V_d = −15.0 Å/ps and the OH group was positioned at one 2.30 Å spacing above the Al (111) slab surface. In model-3 (M−3), V_d = −20.0 Å/ps and all components in O═C─OH functional group were positioned directly at one 2.30 Å spacing above the Al (111) slab surface. The last model was for butanol alcohol reaction with the Al (111) slab: In model-4 (M−4), V_d = −20.0 Å/ps and the OH group was positioned at one 2.30 Å spacing above the Al (111) slab surface.

4.2.1. Dynamic decomposition pathways for butanoic acid on Al (111) slab surface

Figure 14 shows decomposition pathways for M−1, M−2 and M−3 models starting at 300 K. In **Figure 14(a)** for the M−1, at 50 simulation time steps, the O ion in O═C group on butanoic acid molecule began anchoring to the surface in a bi-dentate coordination. However, the OH group did not appear to interact with the surface at this time. At 90 time steps, the O ion in O═C group had dissociated from molecular main piece and was adsorbed onto the surface, with the residual molecular main piece anchoring to the surface through its alkyl-chain. At 200 time steps, the OH group had dissociated from molecular main piece and began interacting with the surface through its O ion. At 310 time steps, the OH group fully dissociated and was adsorbed onto the surface in a uni-dentate coordination. The residual alkyl-chain finally anchored to the surface in a tetra-coordination via its carboxyl C ion, with the O ion (dissociated from the O═C group) adsorbing on the surface in tri-dentate coordination. Note that the temperature of this system increased from 300 to 970 K throughout the whole simulation.

In **Figure 14(b)** for the M−2, at 40 time steps, the OH group interacted with Al (111) surface, resulting in dissociation of one H ion from molecular main piece. Main piece of butanoic acid interacted with the surface in a bi-bridged coordination through its O ions. At 130 time steps,

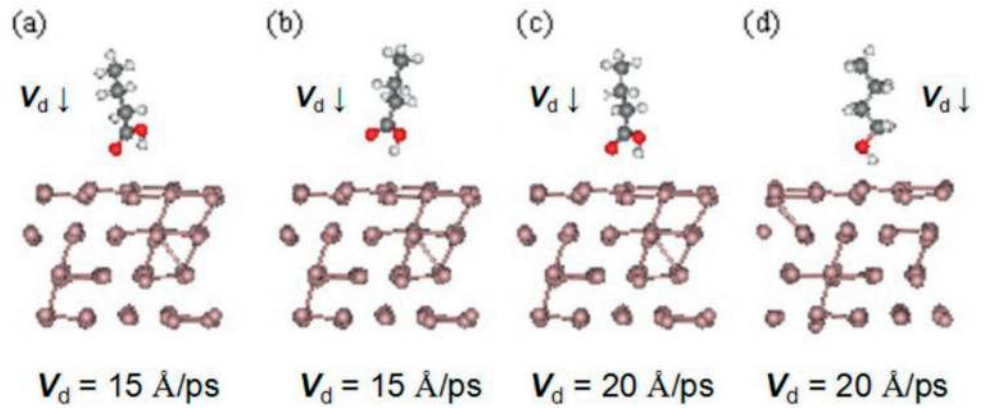

Figure 13. Four initial geometries of butanoic acid and butanol alcohol interactions with Al (111) slab: (a) M−1; (b) M−2; (c) M−3; (d) M−4.

this main piece remained anchoring to the surface. However at 200 time steps, this coordination was becoming uni-dentate as the main piece rebounded the surface under its consistent collisions, and with an Al ion pulled upward by one of O ions in it. At 310 time steps, the fragment in a bi-dentate configuration resembled a soap, i.e., a product of "R─COOM (here "R─ "represented the alkyl-chain and "M" was a metal ion in the surface)" was formed in simulation [33]. Soap formation with fatty acids had been observed in the Al forming process where nominal pressures were in the vicinity of 2.5 times the material flow strength [3, 34]. The temperature of this system increased from 300 to 960 K throughout the whole simulation.

In **Figure 14(c)** for the M−3, at 60 time steps, the O ion in O═C group had dissociated and was subsequently adsorbed in a tri-dentate configuration on Al (111) surface. The same was true for the OH group. The residual alkyl-chain formed bi-dentate and tri-dentate configurations in the order at 100, 150, and 310 time steps throughout the whole simulation. One H ion dissociated from the adsorbed OH group and migrated about the surface. The temperature of this system increased from 300 to 1330 K throughout the whole simulation.

Figure 15 shows the initial evolution of potential energy computed for each of three models in **Figure 14**. In each case, butanoic acid molecule usually began interacting with the surface within 30–50 time steps. The potential energy of each system increased during this time interval so as to overcome the barrier to the adsorption. This energy then decreased as the surface defused molecular consistent impacts and decomposition. Beyond the dip point, the energy increased once again as molecular fragment and its decomposed components in functional

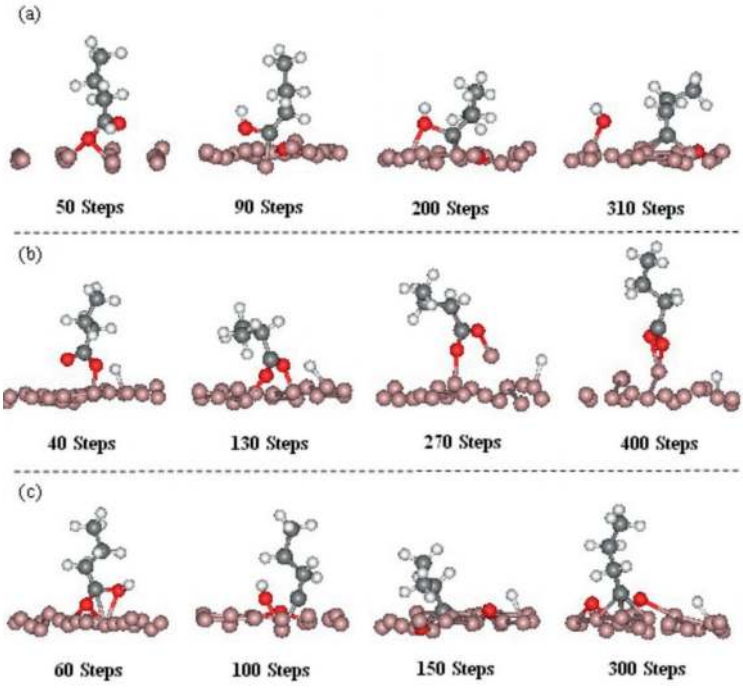

Figure 14. Three models of decomposition pathways starting at 300 K: (a) M−1; (b) M−2 and (c) M−3.

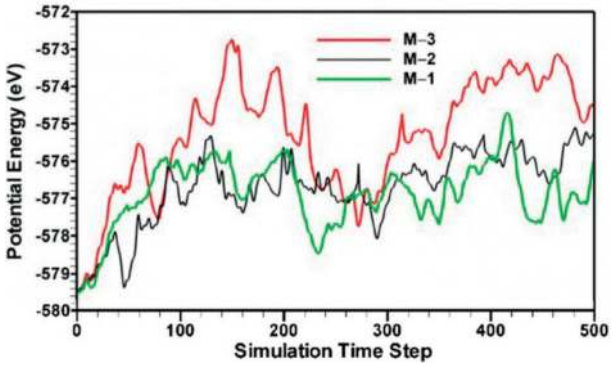

Figure 15. Potential energies of M−1, M−2 and M−3 vs. time steps for butanoic acid decomposition on Al (111) surface.

group re-arranged themselves on the surface. The sharp peaks on M−1 and M−3 curves indicated larger and more rapid exchanges between potential and kinetic energies than were observed in M−2 during the decomposition.

Figure 16 shows potential energies of three models during the first 350 time steps of thermal annealing after their distributions of 500 time steps as shown in **Figure 15**. In **Figure 15**, over this 350 time steps, each curve decreased and ultimately approached an asymptotic value after about 250 time steps. After 350 time steps, the potential energy of M−3 was slightly lower than M−1, but M−2 still had the highest energy level. In addition, our DFT energy minimization found that M−3 was the most stable configuration followed by M−1 and M−2.

4.2.2. Dynamic decomposition pathways for butanol alcohol on Al (111) surface

Figure 17 shows dynamic decomposition pathways for butanol alcohol on Al (111) surface, M–4, starting at 300 K. In **Figure 17**, at 40 time steps, 1 H ion dissociated from the OH group and interacted with an Al ion in the surface. At 100 time steps, molecular fragment was adsorbed on the surface plus a lone H ion moved below the surface. At 250 time steps, molecular fragment

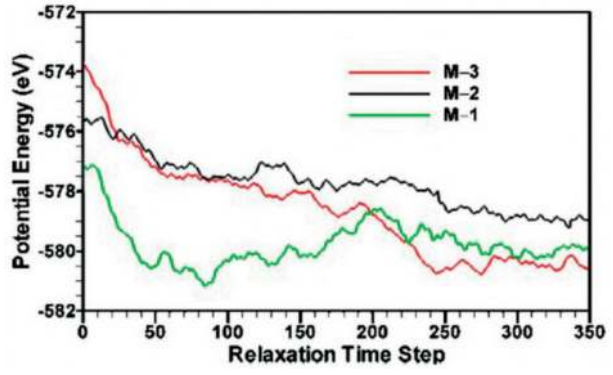

Figure 16. An effect of further annealing at 500 K on potential energies of M−1, M−2 and M−3 for butanoic acid decomposition on Al (111) surface.

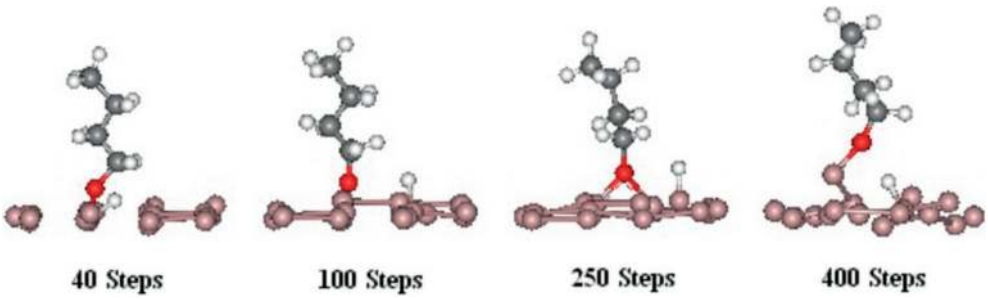

Figure 17. Dynamic decomposition pathways for M–4 starting at 300 K.

evolved its adsorption geometry to a bi-dentate configuration. At 400 time steps, molecular fragment showed up a uni-dentate configuration. Interestingly, during this decomposition, neither bi-dentate nor tri-dentate configuration depicted in above decomposed pieces of butanoic acid were observed in butanol alcohol configurations. Additional AIMD simulations for a butanol alcohol molecule slightly rotated relative to the Al (111) slab also confirmed this observation, see discussions in Section 4.2.3. According to this, we concluded that the decomposition pathway for butanol alcohol just occurred to oxidize the surface by means of its dissociated OH group to form an alcoholate on the surface if other additives were not involved in this reaction.

Figure 18 shows the distribution of potential energy for M–4 starting at 300 K. Here a sharp peak around 40 time steps represented the dissociation of an H ion from molecular main piece. The dip in the curve near 220 time steps was due to the re-arrangement of the decomposed pieces on the surface.

4.2.3. Other decomposition pathways

Other several AIMD simulations were carried out on decomposition pathways with above additive molecules rotating their initial configurations by 180° clockwise (group-1) and 90° counterclockwise (group-2) toward Al (111) surface rather than their functional groups

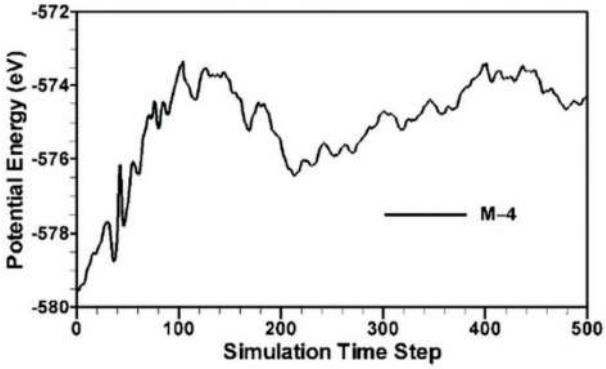

Figure 18. Distribution of potential energy vs. time steps for M–4 starting at 300 K.

facing the surface, respectively. For group-1 with the CH_3 end pointing toward the surface, it initially bounced off the surface without decomposing, but intermediately rotated its functional groups toward the surface when it bounced back the surface. And then, it carried on decomposition pathways discussed in above Sections. For group-2 with the carbon backbones aligning with the surface, it initially bounced off the surface without decomposing, but immediately rotated its functional groups toward the surface when it bounced back the surface. And then it carried on decomposition pathways discussed in above Sections.

Comprehensively, the final thermal equilibration at 500 K for the decomposed species of butanoic acid and butanol alcohol on Al (111) surface indicated that (1) for butanol alcohol decomposed pieces in M-4: a butanol alcoholate was adsorbed on the surface in a uni-dentate coordination with the dissociated H ion adsorbed onto the surface; (2) for butanoic acid decomposed pieces in M−1, M−2 and M−3: residual alkyl-chains usually anchored to the surface in tri-dentate coordination via their carboxyl C ions, with the OH group and dissociated H and O ions interacting with the surface, which were consistent with experimental observations using the X-ray photoelectron spectroscopy (XPS) at temperatures from 300 to 750 K [8].

4.2.4. Conclusions

Simulations of ab-initio molecular dynamics starting at room temperature (300 K) for the decomposed intermediates of aliphatic butanoic acid and butanol alcohol on clean Al (111) surface, indicated that, (1) Initial decomposition pieces of these additive molecules involved attachments of residual alkyl-chains to Al ions in the surface via their oxygen ions; (2) In further decomposition reactions, the remaining alkyl-chains would anchor to the surface via its end C ion, with the complete liberation of oxygen ions or OH group from the carboxyl (O═C─OH) group to oxidize the surface; (3) The remaining alkyl-chains did not participated in reactions with the surface, but may serve as molecular caps to inhibit migrations of corrosive species into the oxide surface, and let these chains accessible react with other general lubricants in base oil, which may form effective boundary thin-films on the surface.

5. Summary

In this chapter, an ab-initio modeling of lubricant reactions with a metal Al (111) surface are comprehensively discussed using density functional theory (DFT) and ab-initio molecular dynamics (AIMD) based upon the DFT, to illuminate some reasonable reaction outputs in this lubrication field. Some main points from discussions may include, without any loss of generality:

1. If ignoring entropy contributions, for the VPA, the best favorable reaction geometries on Al (111) surface were in the order: tri-bridged coordination > bi-bridged coordination > uni-dentate coordination. While for the EA, the best reaction geometries on Al (111) surface were in the order: bi-bridged coordination > uni-dentate coordination.
2. Comparing these two adsorption types, in each of above adsorption geometries, the binding state of VPA on Al (111) surface was always stronger than that for equivalent EA on the surface. The main reason could be due to a more highly reactive functional group of 2(O)─P═O with the surface than that of O─C═O. H ions liberating from molecular main

pieces and adsorbing on the surface, also influenced all the binding states in above. However, the formation of gaseous H_2 molecules by means of H ions desorbed from the surface was more favorable in adsorption ends.

3. Simulations of ab-initio molecular dynamics starting at room temperature (300 K) for the decomposed intermediates of aliphatic butanoic acid and butanol alcohol on clean Al (111) surface, indicated that, (1) Initial decomposition pieces of these molecules involved attachments of residual alkyl-chains to Al ions via their oxygen ions; (2) In further decomposition reactions, the remaining alkyl-chains may anchor to the surface via their end C ions, with complete liberation of oxygen ions on OH groups from carboxyl (O═C─OH) groups to oxidize the surface; (3) The remaining alkyl-chains did not participate in reactions with the surface, but may serve as molecular caps to inhibit migrations of corrosive species into the oxide surface. And, these chains could be accessible to react with other general lubricants in base oil to form effective boundary thin-films on the surface.

Acknowledgements

This work was supported by the National Science Foundation (Grant no.: DMR9619353), USA; the Hebei Province Science and Technology Support Program (Grant no.: 15961006D), the Hebei Province Science and Technology Research Program for Colleges and Universities (Grant no.: QN2016206), and the Start-up Fund of Doctoral Research at North China Institute of Aerospace Engineering (Grant no.: BKY201405), China.

Author details

Jun Zhong

Address all correspondence to: settings83@hotmail.com

North China Institute of Aerospace Engineering, Langfang, China

References

[1] Totten G, Liang H. Surface Modification and Mechanisms: Friction, Stress and Reaction Engineering. New York: CRC Press; 2004. p. 765. ISBN # 0-8247-4872-7

[2] Sutcliffe M, Combarieu R, Montmitonnet P. Tribology of plane strain compression tests on aluminium strip using ToF-SIMS analysis of transfer films. Wear. 2003;**254**:65-79. DOI: 10.1016/S0043-1648(02)00295-8

[3] Opalka SM, Hector LG Jr, Schmid S, Reich RA. Boundary additive effect on abrasive wear during single asperity plowing of a 3004 aluminum alloy. Journal of Tribology 1999; **121**:384-393. DOI: 10.1115/1.2833951

[4] Coast R, Pikus M, Henriksen PN, Nitowski GA. A vibrational spectroscopic comparison of vinyl-triethoxysilane and vinyl-phosphonic acid adsorbed on oxidized

aluminum. Journal of Adhesion Science and Technology. 1996;(2):101-121. DOI: 10.1163/156856196X00805

[5] Ramsier RD, Henriksen PN, Gent AN. Adsorption of phosphorus acids on alumina. Surface Science. 1988;**203**:72-88. DOI: 10.1016/0039-6028(88)90195-1

[6] Chen JG, Crowell JE, Yates JT Jr. An EELS and TPD study of the adsorption and decomposition of acetic acid on the Al (111) surface. Surface Science 1986;**172**:733-753. DOI: 10.1016/0039-6028(86)90509-1

[7] Crowell JE, Chen JG, Yates JT Jr. The adsorption and decomposition of carboxylic acids on Al (111). Journal of Electron Spectroscopy and Related Phenomena 1986;**39**:97-106. DOI: 10.1016/0368-2048(86)85037-X

[8] Underhill R, Timsit RS. Interaction of aliphatic acids and alcohols with aluminum surfaces. Journal of Vacancy Science and Technology A. 1992;**10**:2767-2774. DOI: 10.1116/1.577908

[9] Zhong J, Adams JB. Adsorption and decomposition pathways of vinyl phosphonic and ethanoic acids on the Al (111) surface: A density functional analysis. Journal of Physical Chemistry C. 2007;**111**:7366-7375. DOI: 10.1021/jp0667487

[10] Available from: Website: http://environmentalchemistry.com/yogi/periodic/crystal.html

[11] Kresse G. VASP the GUIDE. http://cms.mpi.univie.ac.at/vasp/vasp/vasp.html

[12] Kresse G, Hafner J. Norm-conserving and ultrasoft pseudopotentials for first-row and transition elements. Journal of Physics: Condensed Matter. 1994;**6**:8245-8258. DOI: 10.1088/0953-8984/6/40/015

[13] Kresse G, Furthmüller J. Efficient iterative schemes for ab initio total-energy calculations using a plane-wave basis set. Physical Review B. 1996;**54**:11169-11186. DOI: 10.1103/PhysRevB.54.11169

[14] Jiang Y, Adams JB. First principle calculations of benzotriazole adsorption onto clean Cu (111). Surface Science. 2003;**529**:428-442. DOI: 10.1016/S0039-6028(03)00277-2

[15] Hector LG Jr, Adams JB, Siegel DJ. Investigation of vinyl phosphonic acid/hydroxylated α-Al_2O_3 (0001) reaction enthalpies. Surface Science 2001;**494**:1-20. DOI: 10.1016/S0039-6028(01)01387-5

[16] Hohenberg P, Kohn W. Inhomogeneous electron gas. Physical Review. 1964;**136**:B864-B871. DOI: 10.1103/PhysRev.136.B864

[17] Kohn W, Sham LJ. Self-consistent equations including exchange and correlation effects. Physical Review. 1965;**140**:A1133-A1138. DOI: 10.1103/PhysRev.140.A1133

[18] Jones RO, Gunnarsson O. The density functional formalism, its applications and prospects. Reviews of Modern Physics. 1989;**61**:689-746. DOI: 10.1103/RevModPhys.61.689

[19] Blöchl PE. Projector augmented-wave method. Physical Review B. 1994;**50**:17953-17979. DOI: 10.1103/PhysRevB.50.17953

[20] Perdew JP, Wang Y. Accurate and simple density functional for the electronic exchange energy: Generalized gradient approximation. Physical Review B. 1986;**33**:8800(R)-8802(R). DOI: 10.1103/PhysRevB.33.8800. Erratum: DOI: 10.1103/PhysRevB.40.3399

[21] Perdew JP, Chevary JA, Fiolhais C. Atoms, molecules, solids, and surfaces: Applications of the generalized gradient approximation for exchange and correlation. Physical Review B. 1992;**46**:6671-6687. DOI: 10.1103/PhysRevB.46.6671

[22] Murnaghan FD. The compressibility of media under extreme pressures. Proceedings of the National Academy of Sciences of the United States of America. 1944;**30**:244-247. DOI: http://www.pnas.org/content/30/9/244.full.pdf

[23] Monkhorst HJ, Pack JD. Special points for brillouin-zone integrations. Physical Review B. 1976;**13**:5188-5192. DOI: 10.1103/PhysRevB.13.5188

[24] Vanderbilt D. Soft self-consistent pseudopotentials in a generalized eigenvalue formalism. Physical Review B. 1990;**41**:7892(R)-7895(R). DOI: 10.1103/PhysRevB.41.7892

[25] Kroes GJ, Baerends EJ, Mowrey RC. Six-dimensional quantum dynamics of dissociative chemisorption of (v = 0, j = 0) H_2 on Cu (100). Physical Review Letters. 1997;**78**:3583-3586. DOI: 10.1103/PhysRevLett.78.3583. Erratum: DOI: 10.1103/PhysRevLett.81.4781

[26] Tuma C, Sauer J. Treating dispersion effects in extended systems by hybrid MP2: DFT calculations–protonation of isobutene in zeolite ferrierite. Physical Chemistry Chemical Physics. 2006;**8**:3955-3965. DOI: 10.1039/B608262A

[27] Nieto P, Pijper E, Barredo D, Laurent G, Olsen RA, Baerends EJ, Kroes GJ, Farıas D. Reactive and nonreactive scattering of H_2 from a metal surface is electronically adiabatic. Science. 2006;**312**:86-89. DOI: 10.1126/science.112305

[28] Zhong J, Hector LG Jr, Adams JB. Dynamic decomposition of aliphatic molecules on Al (111) from ab initio molecular dynamics. Physical Review B. 2009;**79**:125419. DOI: 10.1103/PhysRevB.79.125419

[29] Heermann DW. Computer Simulation Method in Theoretical Physics. 2nd ed. Berlin: Springer-Verlag; 1990. p. 145. ISBN-13: 978-3540522102

[30] Kojima S, Yokoyama A, Komatsu M, Kiritani M. High-speed deformation of aluminum by cold rolling. Materials Science and Engineering A. 2003;**350**:81-85. DOI: 10.1016/S0921-5093(02)00698-6

[31] Jayatilaka D, Grimwood D. Electron localization functions obtained from X-ray constrained Hartree-Fock wavefunctions for molecular crystals of ammonia, urea and alloxan. Acta Crystallography Section A - Foundations and Advances. 2004;**A60**:111-119. DOI: 10.1107/S0108767303029350

[32] Pauling LC. The Nature of the Chemical Bond. 3rd ed. New York: Cornell University Press; 1960. p. 664. ISBN-10: 0801403332

[33] Rao KB, Jena P, Burkart S, Gantefor G, Seifert G. AlH_3 and Al_2H_6: Magic clusters with unmagical properties. Physical Review Letters. 2001;**86**:692-695. DOI: 10.1103/PhysRevLett.86.692

[34] Totten GE. Handbook of Lubrication and Tribology: Volume 1 Application and Maintenance. 2nd ed. New York: CRC Press; 2006. p. 1224. ISBN: 9780849320958 - CAT # 2095